10 Application of Thermochronology to Geologic Problems: Bedrock and Detrital Approaches

Marco G. Malusà and Paul G. Fitzgerald

Abstract

Low-temperature thermochronology can be applied to a wide range of geologic problems. In this chapter, we provide an overview of different approaches, underlying assumptions and suitable sampling strategies for bedrock and detrital thermochronologic analyses, with particular emphasis on the fission-track (FT) method. Approaches to bedrock thermochronology are dependent on the goals of the project and the regional geologic setting, and include application of: (i) multiple methods (e.g., FT, (U–Th)/He and U–Pb) on various mineral phases (e.g., apatite and zircon) from the same sample, (ii) single methods on multiple samples collected over significant relief or across a geographic region (regional approach) or (iii) multiple methods on multiple samples. The cooling history of rock samples can be used to constrain exhumation paths and provides thermochronologic markers to determine fault offset, timing of deformation and virtual tectonic configurations above the present-day topography. Detrital samples can be used to constrain erosion patterns of sediment source regions on both short-term (10^3–10^5 yr) and long-term (10^6–10^8 yr) timescales, and their evolution through time. The full potential of the detrital thermochronology approach is best exploited by the integrated analysis of samples collected from a stratigraphic succession, samples of modern sediment and independent mineral fertility determinations.

M. G. Malusà (✉)
Department of Earth and Environmental Sciences, University of Milano-Bicocca, Piazza delle Scienza 4, 20126 Milan, Italy
e-mail: marco.malusa@unimib.it

P. G. Fitzgerald
Department of Earth Sciences, Syracuse University, Syracuse, NY 13244, USA

10.1 Bedrock Thermochronology Studies

Low-temperature thermochronology studies fall into two general categories: those where samples are collected from bedrock and those where samples are essentially detrital. Within each of these two groups there are also natural subdivisions such as: for bedrock studies, applying a key-locality/outcrop approach (e.g., collecting over significant relief (the vertical profile approach) to determine age-elevation relationships) and/or a more regional sampling approach, all of which are dependent on the objectives of the study, the available geologic information, if other methods are also to be applied and if subsequent thermal modelling might also be applied. The geologic problem being addressed ideally helps shape the sampling strategy. Typically, the part of a study that has the longest longevity is the data itself. For example, modelling methods change and evolve, but the data remains the same, all things being equal.

10.1.1 Multiple-Method Versus Age-Elevation Approach for the Analysis of Exhumation Rates

When bedrock samples are collected on a regional basis, an exhumation rate for single samples may be estimated by assuming that the ages represent closure temperature (T_c) ages, and by assuming (or knowing) the paleogeothermal gradient to calculate depth to T_c. Hence, the depth divided by the ages yields an apparent exhumation rate (e.g., Reiners and Brandon 2006). This approach is not applied quite so much to basement samples, especially if inverse thermal models are available (Chap. 3, Ketcham 2018). However, it still remains the fundamental approach for many detrital thermochronology studies (e.g., Garver et al. 1999) (see Sect. 10.2).

More common approaches in studies utilising low-temperature thermochronology on bedrock samples involve the combination of multiple methods with different T_c, and sampling along vertical profiles (Fig. 10.1). The

M. G. Malusà and P. G. Fitzgerald (eds.), *Fission-Track Thermochronology and its Application to Geology*,
Springer Textbooks in Earth Sciences, Geography and Environment, https://doi.org/10.1007/978-3-319-89421-8_10

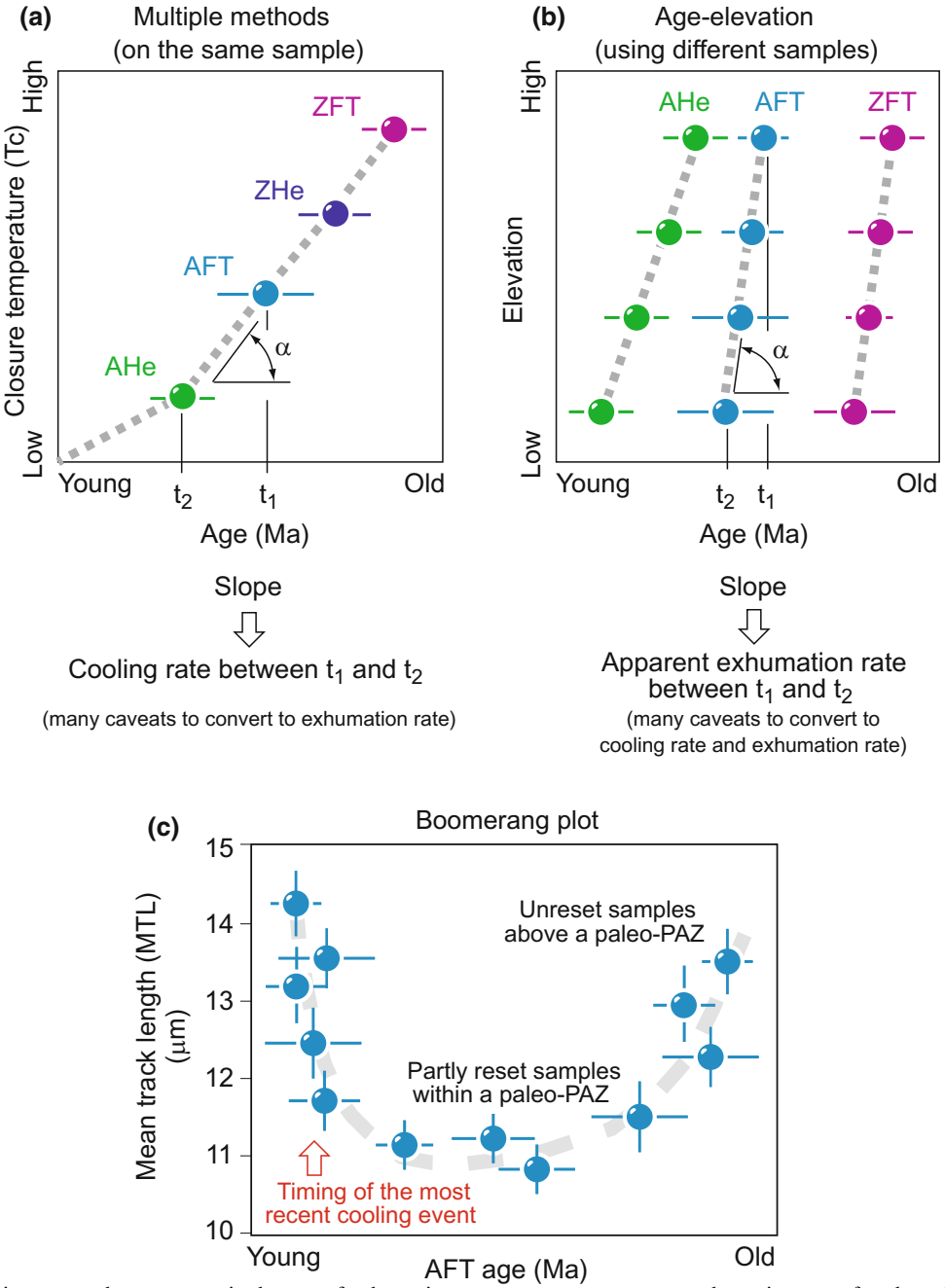

Fig. 10.1 Alternative approaches to constrain the rate of exhumation from bedrock samples. **a** Multiple-method approach. It is based on the analysis of different mineral/systems with progressively lower closure temperatures (T_c) on the same sample. The gradient of the slope in the diagram is a function of the average cooling rate between time t_1 and t_2. The paleogeothermal gradient during cooling has to be independently known in order to convert this average cooling rate to an average exhumation rate. **b** Age-elevation (vertical profile) approach. It is based on the analysis of an array of samples collected from top-to-bottom of significant relief and utilising the same dating method. When data are plotted on an age-elevation diagram, the gradient of the slope provides an apparent average exhumation rate for the whole time interval between the age yielded by the uppermost (t_1) and the lowermost (t_2) samples, or for individual discernable portions of the age-elevation profile that may have different slopes. Multiple methods can, and often are applied to the same array of samples to constrain the exhumation history over a longer time interval. **c** Boomerang plot that can be used to detect partly reset or unreset samples lying within or above a paleo-PAZ, and determine the onset of the most recent cooling event (based on Gallagher and Brown 1997). Acronyms: AFT, apatite fission track; AHe, apatite (U–Th)/He; ZFT, zircon fission track; ZHe, zircon (U–Th)/He

multiple-method approach (Fig. 10.1a) is based on the analysis of different thermochronologic systems in minerals retrieved from the same sample (e.g., Wagner et al. 1977; Hurford 1986; Moore and England 2001). Different mineral/systems with progressively lower T_c generally yield progressively younger thermochronologic ages, constraining a cooling history that is generally related to the exhumation of the sample towards the Earth's surface. In a diagram showing T_c versus the thermochronologic ages yielded by the analysed sample (Fig. 10.1a), the gradient of the slope is a function of the cooling rate in the selected time interval and is steeper for faster cooling. Converting this average cooling rate into an exhumation rate is not straightforward, as the paleogeothermal gradient during cooling has to be independently known (see Chap. 8, Malusà and Fitzgerald 2018). The multiple-method approach is generally more applicable for samples that have cooled across a wider temperature range (i.e., several hundreds of °C), which makes this approach suitable for the analysis of rocks exhumed from greater depths (see Chap. 13, Baldwin et al. 2018). Higher temperature thermochronologic methods are slower to respond to changes in exhumation rates (Moore and England 2001). Thus, if there is a step-wise increase in erosion rates at the surface, different methods on the same sample may give the appearance of a gradually increasing erosion rate with time as the T_c isotherms migrate at different rates to their new steady-state depths.

The *age-elevation (vertical profile) approach* is based on the analysis of an array of samples collected across a significant elevation range (and a short horizontal distance) employing the same dating method (e.g., Wagner and Reimer 1972; Naeser et al. 1983; Gleadow and Fitzgerald 1987; Fitzgerald and Gleadow 1988, 1990; Fitzgerald et al. 1995; Ruiz et al. 2009). During exhumation from depths greater than the T_c isothermal surface, samples collected from higher elevations cross the T_c isothermal surface before those from lower elevations, leading to a normal age-elevation relationship (i.e., samples collected at higher elevation have older ages). The gradient of the slope in an age-elevation diagram provides an apparent average exhumation rate for the time interval between the age yielded by the uppermost sample (t_1 in Fig. 10.1b) and the age yielded by the lowermost one (t_2 in Fig. 10.1b). The slope is generally steeper for faster exhumation rates. This estimate does not require any explicit assumption about the paleogeothermal gradient, but converting an apparent exhumation rate to a true exhumation rate using the age-elevation approach is not straightforward and requires a careful analysis of the relationships between the topography and the thermal reference frame (see Chap. 9, Fitzgerald and Malusà 2018).

An important assumption underlying the age-elevation approach is that the spatial relationships between samples have remained unchanged since the time of exhumation. Therefore, this approach should not be applied, for example, across faults that may have modified these original relationships: Samples from different fault blocks must be considered separately. Conversely, this approach can be used to detect faults between samples with contrasting or unexpected ages. Additionally, the difference in elevation between the lowest and the highest samples should be sufficiently large to allow a significant spread in thermochronologic ages, at least compared to the standard error associated with each age. This is particularly important for rapidly exhuming areas, where thermochronologic ages tend to be invariant with elevation. The most favourable conditions for a successful application of the age-elevation method are thus represented by a combination of high topographic relief and relatively slow exhumation rates, which allows for a larger spread of thermochronologic ages in the array of analysed samples. However, the time interval constrained by the age-elevation approach using one dating method only (t_1 to t_2 in Fig. 10.1b) may be quite short. In order to constrain the exhumation history over a longer time interval, multiple methods may be applied to the same array of samples (Fig. 10.1b). The time intervals constrained by different thermochronologic methods may either overlap, thus providing complementary constraints to specific segments of the exhumation path, or leave unconstrained time intervals between different methods, as often observed when the relief covered by samples is not sufficiently large. Different age-elevation slopes may be recorded for different thermochronologic methods even if the same exhumation rate is ongoing. This is because of the effects of topography and the bending of isothermal surfaces under ridges and valleys (e.g., Stüwe et al. 1994; Mancktelow and Grasemann 1997; Braun 2002), which can be investigated by suitable sampling strategies as discussed in Chaps. 9 (Fitzgerald and Malusà 2018) and 19 (Schildgen and van der Beek 2018).

The vertical spacing between samples is also important, and should be sufficiently small to highlight any change in slope, either ascribed to variations in exhumation rates or to the presence of a paleo-PAZ (Partial Annealing Zone) (see Chap. 9, Fitzgerald and Malusà 2018). For the calculation of an apparent exhumation rate, thermochronologic ages yielded by partly reset or unreset samples, i.e., by samples collected within or above a paleo-PAZ (as revealed, e.g., by grain age over dispersion or by confined track-length distributions) should not be included (see Chap. 6, Vermeesch 2018; Chap. 9, Fitzgerald and Malusà 2018).

Plots displaying the measured FT age against the mean track length (MTL) provide a useful approach to visualise the occurrence of partly reset or unreset samples lying within or above a paleo-PAZ (Fig. 10.1c). Samples collected from a range of initial paleodepths in a region that has undergone broadly coeval cooling will define a concave-up

"boomerang" shape (Green 1986). This boomerang trend includes: (i) old ages with long MTLs corresponding to samples that have spent most time above the PAZ; (ii) intermediate ages with the shortest MTLs, corresponding to samples that have spent most time within the PAZ; and (iii) young ages with long MTLs that have experienced the highest initial paleotemperatures. The timing of the most recent cooling event is constrained by the transition from samples with "intermediate" FT ages and MTLs in the 12–13 μm range to samples with younger FT ages and MTLs in the range of 14–15 μm (e.g., Brown et al. 1994; Fitzgerald 1994; Gallagher and Brown 1997; Hendriks et al. 2007). These latter samples can be used to estimate an apparent exhumation rate using the age-elevation approach, provided these samples are collected from the same fault block and fulfil the criteria described in Chap. 9 (Fitzgerald and Malusà 2018).

10.1.2 Virtual Configuration of Rock Units by FT Thermochronology

Low-temperature thermochronology can also be used to envisage a paleo-thermal structure and infer the original thickness of overburden, which may include partly eroded stratigraphic successions or eroded thrust sheets (Fig. 10.2a–c). This is one application of *FT stratigraphy*, with "stratigraphy" represented by the variation of age with elevation or depth (in case of boreholes) (e.g., Brown 1991).

The radial plots in Fig. 10.2a illustrate the grain-age distributions normally expected in samples of sedimentary rocks collected at increasing depths down a borehole in a sedimentary basin. Samples that have experienced minor burial and have remained above the PAZ of the chosen thermochronologic system (black circles in Fig. 10.2a) will show either unimodal or polymodal grain-age distributions, with grain-age populations systematically older than the stratigraphic age of the sample. Samples that have experienced burial within the PAZ (grey circles in Fig. 10.2a) will display partly reset FT ages that with increasing temperature become progressively younger than the stratigraphic age of the sample. Samples located below the PAZ, i.e., at higher temperatures (white circles in Fig. 10.2a), will yield a zero FT age because the fission tracks have been totally annealed.

Subsequent to burial, and following rapid exhumation to the surface, let us now examine age/length trends on this exhumed stratigraphic succession (Fig. 10.2b). Sedimentary rocks originally located below the PAZ (white circles in Fig. 10.2b) yield unimodal grain-age distributions with a central age that is equal to, or slightly younger (although often not much younger) than this rapid exhumation. Samples that have experienced burial within the PAZ (grey circles in Fig. 10.2b) will display FT ages ranging between the stratigraphic age of the sample and the time of exhumation. The timing of the transition between the completely reset and the partially reset samples typically marks the timing of the initiation of more rapid cooling and exhumation. Samples that have remained above the PAZ will provide information on older exhumation/crystallisation events in the sediment source areas, which can be investigated by using the detrital thermochronology approaches described in Sect. 10.2 (see also Chap. 14, Carter 2018; Chap. 15, Bernet 2018; Chap. 16, Malusà 2018 and Chap. 17, Fitzgerald et al. 2018 for more details). Clues for the interpretation of partially reset detrital samples can be found in Brandon et al. (1998) and in Chap. 18 (Schneider and Issler 2018).

The occurrence of partly or fully reset detrital samples in the uppermost levels of a stratigraphic sequence provides evidence of overburden removal by denudation (Fig. 10.2b). When the paleogeothermal gradient is reasonably assumed or independently known, the FT stratigraphy approach provides a useful way to estimate the depth of erosional denudation and the virtual configuration of eroded rock units above the present-day topography (Fig. 10.2c). Examples include studies in the central Alaska Range to estimate the amount of rock present above the summit of Denali prior to the onset of rapid exhumation in the Late Miocene (Fitzgerald et al. 1995, see also Chap. 9, Fitzgerald and Malusà 2018); in the Apennines to infer the virtual configuration of the Ligurian wedge on top of the Adriatic foredeep units (Zattin et al. 2002); in eastern Anti-Atlas to infer the past configuration of the Variscan belt on top of the Precambrian basement of the West African Craton (Malusà et al. 2007); in the Canadian Cordillera to infer the initial thickness of the Lewis thrust sheet (Feinstein et al. 2007); in SE France to infer the virtual configuration of the Alpine nappes on top of the Paleogene sedimentary succession of the European foreland (Labaume et al. 2008; Schwartz et al. 2017). The number of samples required for a reliable reconstruction of these virtual configurations is often quite high, and datasets will ideally include samples from different levels of the stratigraphic succession.

10.1.3 The Analysis of Fault Offsets Using Thermochronologic Markers

Low-temperature thermochronology often provides time constraints on fault activity and markers for the analysis of fault offsets (e.g., Gleadow and Fitzgerald 1987; Gessner et al. 2001; Raab et al. 2002; Fitzgerald et al. 2009; Niemi

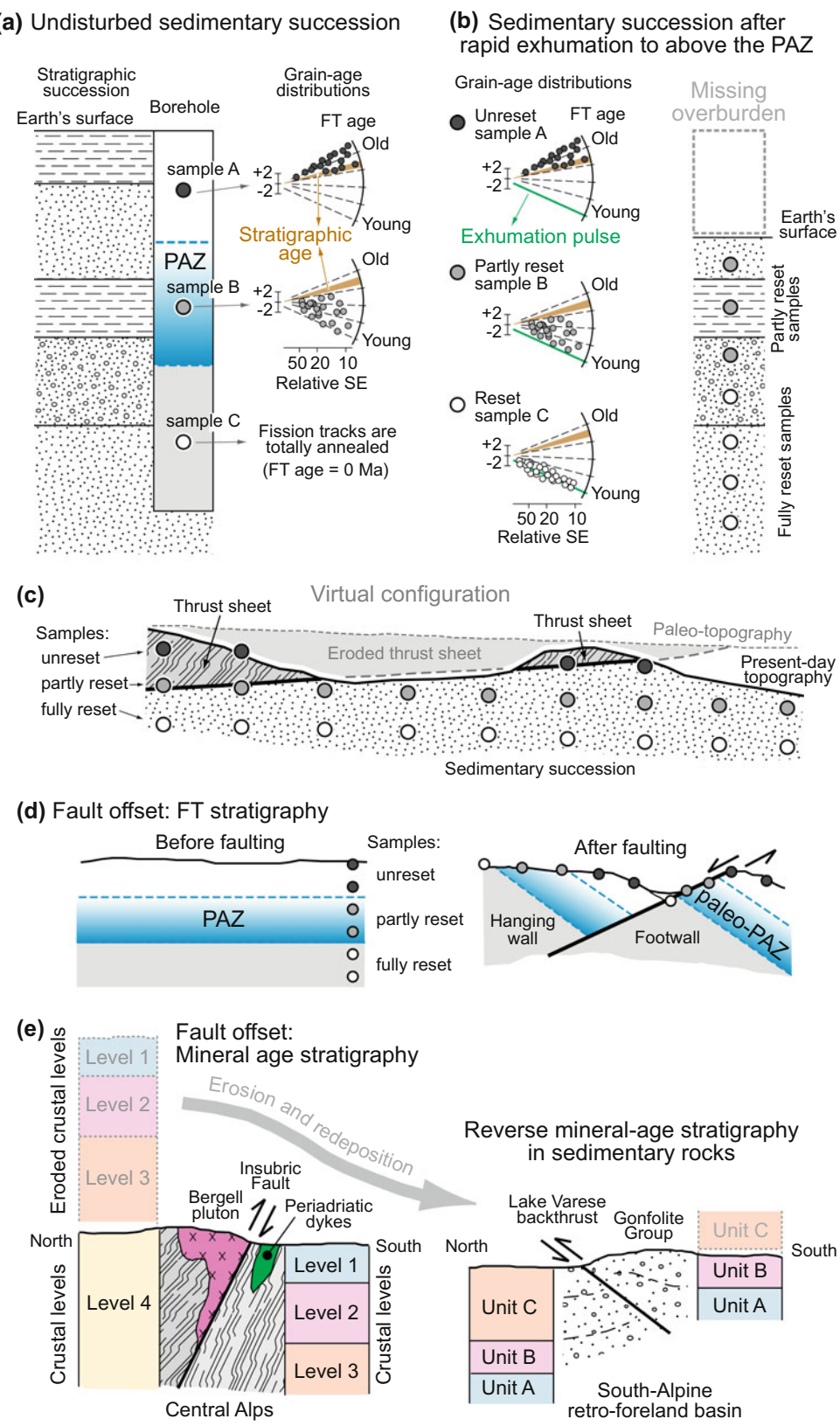

Fig. 10.2 Analysis of virtual geologic configurations and fault offsets using thermochronologic markers. **a** Grain-age distributions expected for increasing depths down a borehole in a sedimentary basin: samples that have remained above the PAZ of the chosen thermochronologic system (black circles) show grain ages systematically older than the stratigraphic age of the sample; samples that have experienced burial within the PAZ (grey circles) display partly reset (annealed) FT ages that are younger than the stratigraphic age of the sample; samples located below the PAZ (white circles) yield zero FT ages because fission tracks are totally annealed. **b** The same stratigraphic succession after exhumation. Sedimentary rocks originally located below the PAZ (white circles) display unimodal grain-age distributions with a central age that records the time of last exhumation. Samples that have experienced burial within the PAZ (grey circles) display FT ages ranging between the stratigraphic age and the time of last exhumation. The occurrence of partly or fully reset samples in the uppermost levels of a stratigraphic succession provides evidence of overburden removal by erosion or tectonic processes. **c** Reconstructed configuration of eroded rock units based on the distribution of unreset, partly annealed and fully reset samples in a modern landscape. **d** Analysis of fault offset by FT stratigraphy (diagram is modified from Stockli et al. 2002). **e** Analysis of fault offsets by mineral-age and reverse mineral-age stratigraphy (based on Malusà et al. 2011); numbers refer to hypothetical crustal levels and letters refer to hypothetical stratigraphic units (see Chap. 16, Malusà 2018 for more details)

et al. 2013; Ksienzyk et al. 2014; Balestrieri et al. 2016, and Chap. 11, Foster 2018). Such markers are particularly useful in case of monotonous sequences of sedimentary, magmatic and metamorphic rocks, where geologic markers are absent, and in regions of poor outcrop where other markers are not available (e.g., forested or glaciated areas). Thermochronologic markers may include a paleo-PAZ and FT stratigraphy (Fig. 10.2d) (e.g., Brown 1991; Fitzgerald 1992; Foster et al. 1993; Bigot-Cormier et al. 2000; Stockli et al. 2002; Thiede et al. 2006; Richardson et al. 2008; Fitzgerald et al. 2009; Kounov et al. 2009; Miller et al. 2010), which potentially constrain fault activity in the uppermost few kilometres of the crust (Chap. 11, Foster 2018). Both the multiple-method and age-elevation approaches described in Sect. 10.1.1, when applied to distinct crustal blocks, are potentially able to highlight episodes of differential exhumation across major faults, thus constraining the age of fault activity (e.g., Gleadow and Fitzgerald 1987; Fitzgerald 1992, 1994; Foster et al. 1993; Foster and Gleadow 1996; Viola et al. 2001; West and Roden-Tice 2003; Malusà et al. 2005, 2009a; Niemi et al. 2013; Riccio et al. 2014). Given the precision of the ages on either side of the fault, which is typically ±5% (±1σ) for apatite FT (AFT) ages, faults with small offsets will not be revealed. Whether a fault offset is revealed often depends on the age-elevation relationship. If the slope is shallow (ages vary considerably with change in elevation) age-offsets due to faulting are often revealed, whereas when the slope is steep (ages do not vary much with elevation) faults are typically not revealed, as there is little age-offset across the fault unless the vertical fault offset is extremely large (i.e., several kilometres). Constraints on the fault offsets are usually more reliable when the local FT stratigraphy is well documented and multiple samples (if possible collected over a significant elevation range on either side of the fault to confirm the local age-elevation slope) are used. Observations of age trends such as these can be integrated by information provided by temperature-time paths, based on the modelling of confined track lengths in samples collected on the opposite sides of the fault (e.g., Thomson 2002; Balestrieri et al. 2016). If the paleogeothermal gradient is independently known, the multiple-method analysis of distinct fault blocks may provide reliable estimates of fault throws accommodated through time (e.g., Malusà et al. 2006).

In a well-known example, Fitzgerald (1992) tested the FT stratigraphy approach across the Transantarctic Mountain Front in the Dry Valleys area where the location and offset of normal faults are well-delineated by step-faulted horizontal dolerite sills (see also Chap. 9, Fitzgerald and Malusà 2018). There, reconstruction of the ~100 Ma isochron from samples collected systematically along the faulted ridge was used to reliably document fault offsets as small as ~200 m. This was, however, an ideal situation where the slope of the age-elevation relationship (an exhumed PAZ) was ~15 m/Myr; thus, an offset of 300–400 m represents a discernable age difference of 20–25 Ma. Miller et al. (2010) undertook a similar study across the Transantarctic Mountain Front at Cape Surprise near the Shackleton Glacier, distinguishing between the presence of one master fault with offset of ~5 km or a series of smaller faults, as it proved to be.

Fault offsets can be also constrained by *mineral-age stratigraphy* (Malusà et al. 2011), which is based on the specific combinations of crystallisation and exhumation ages that are yielded by different thermochronometers (and minerals) at different depths in the crust (see Chap. 8, Malusà and Fitzgerald 2018, their Fig. 8.7). Such combinations allow one to define, on a thermochronologic basis, a stratigraphy of increasingly deeper crustal levels (Levels 1–4 in Fig. 10.2e) that may be able to constrain fault offsets in homogeneous rock sequences. Mineral-age stratigraphy can be particularly useful in cases where plutonic rocks dominate the geology (Fig. 10.2e). Use of mineral-age stratigraphy may also, when compared to FT stratigraphy, constrain greater offsets across faults because the data spans a greater temperature interval. In the case of the Insubric Fault in the European Alps, this approach provides evidence of >10–15 km fault offset of the uplifted crustal block north of the fault, relative to the downthrown southern side. On the north, the Periadriatic Bergell/Bregaglia pluton, emplaced in the Oligocene, is now unroofed down to a crustal level that was lying below the T_c of the K–Ar system on biotite at the time of intrusion (level 4 in Fig. 10.2e). This is attested by biotite K–Ar ages (26–21 Ma, Villa and von Blanckenburg 1991) that are much younger than the intrusion age provided by zircon U–Pb dating (30 ± 2 Ma, Oberli et al. 2004). In comparison, the block south of the Insubric Fault has Periadriatic dykes now exposed at the surface. These dykes show zircon U–Pb and AFT ages, yielding two clusters at 42–39 Ma and 35–34 Ma, that are generally indistinguishable within error (D'Adda et al. 2011; Malusà et al. 2011; Zanchetta et al. 2015), because they were emplaced at crustal levels lying within or just below the AFT PAZ at the time of intrusion (level 1 or 2 in Fig. 10.2e). These constraints integrate previous estimates of fault offsets based on the multiple-method approach (Hurford 1986).

The mineral-age stratigraphy observed in an orogen undergoing erosion may subsequently be observed as a "reverse" age stratigraphy in sedimentary basins fed from that eroding source. This reverse age trend can thus be used as a marker to detect tectonic repetitions and fault offsets in the absence of other stratigraphic markers (Fig. 10.2e, right panel). For example, application of this approach to the Oligocene–Miocene Gonfolite Group derived from the erosion of the Bergell pluton (Wagner et al. 1979; Bernoulli et al. 1989) provided evidence for a major and previously undetected thrust fault in the Gonfolite Group (Lake Varese backthrust in Fig. 10.2e) (Malusà et al. 2011).

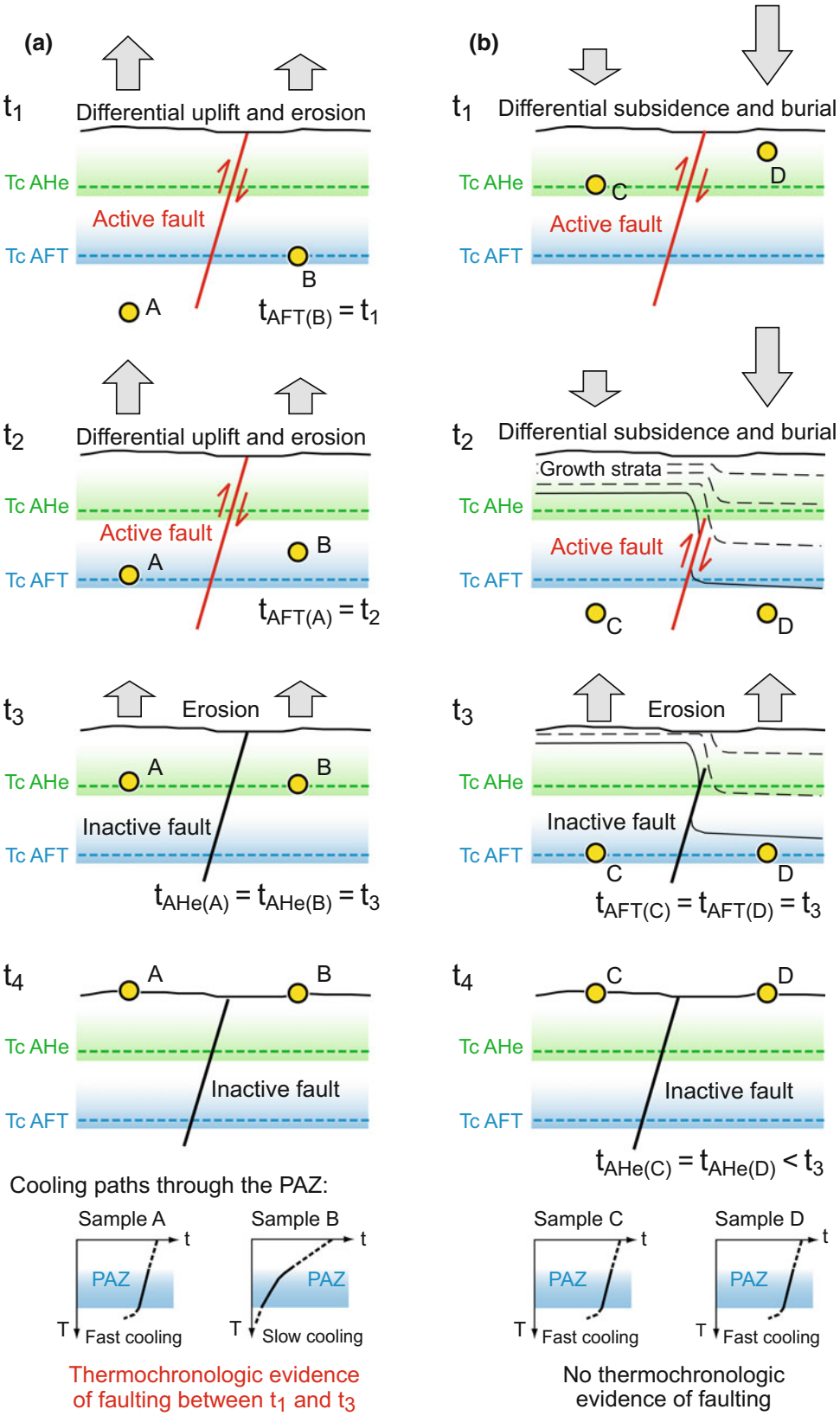

Fig. 10.3 Time constraints to fault activity based on thermochronologic analysis. **a** Reverse fault (in red) accommodating differential uplift and exhumation before time t_3. The time of faulting is successfully constrained by AFT and AHe analyses in rock samples A and B collected on the opposite sides of the fault, and by modelling of confined track-length distributions. AHe ages in samples A and B are equal to t_3, and indistinguishable across the fault, which is in line with the cessation of fault activity not later than time t_3. **b** Reverse fault accommodating differential subsidence before time t_3, when the analysed samples C and D are at similar crustal level as samples A and B. AFT and AHe analyses of samples C and D provide no direct constraint to the age of faulting, whereas higher T_c thermochronometers would record events much older than t_1. The effects of advection on isothermal surfaces are not included for the sake of simplicity

Thermochronologic analyses across major faults can ideally constrain the timing of deformation thanks to a detailed reconstruction of the differential exhumation paths experienced by different fault blocks through time. In the example of Fig. 10.3 (left panel), the activity of a reverse fault before time t_3 is well constrained by apatite (U–Th)/He (AHe) and AFT analyses in rock samples A and B collected on the opposite sides of the fault, and by inverse modelling using age and confined track-length data from the same samples. AHe ages in samples A and B are equal to t_3, and indistinguishable across the fault, which is in line with the cessation of fault activity not later than time t_3. Importantly, there is usually only clear thermochronologic evidence for fault offset when faults accommodate differential exhumation (Fig. 10.3a), but such evidence is not observed when faults accommodate differential subsidence (Fig. 10.3b). Such an observation, with respect to cooling rather than exhumation/subsidence, has long been established (e.g., Green et al. 1989). The situation of faults accommodating differential subsidence is typical, for instance, of rapidly subsiding foreland basins such as the Po Plain north of the Apennines (Pieri and Groppi 1981). In Fig. 10.3b, the reverse fault indicated in red is active at the same time interval as the fault in Fig. 10.3a, and when the analysed samples (C and D) at the time of faulting were at the same crustal level as samples A and B. However, the thermochronologic analysis of samples C and D provides no useful constraint on the timing of deformation.

In the case where fault motion is dominantly strike-slip, differential exhumation between fault blocks is usually minimal. As a consequence, thermochronologic evidence for faulting along strike-slip systems is generally observed particularly at restraining bends or step-overs, or where there is transpression. Well-known examples of these situations have been documented along the Denali Fault (e.g., Riccio et al. 2014), the San Andreas Fault (e.g., Niemi et al. 2013) and the Alpine Fault (e.g., Herman et al. 2007; Warren-Smith et al. 2016).

Sampling strategies to provide timing constraints on fault activity, and markers for the analysis of fault offsets (see Chap. 11, Foster 2018), must be designed to minimise the bias arising from the complexity of isotherms close to major faults (see Chap. 8, Malusà and Fitzgerald 2018). Large (crustally penetrative) faults are most likely to have a thermal perturbation (Ehlers 2005), and for these faults, it is advisable to collect samples tens to hundreds of metres from the main deformation zone. In contrast, some studies seek to exploit the thermal perturbation along the faults to constrain the fault activity (Tagami et al. 2001; Murakami and Tagami 2004), and samples are best collected from a closely spaced array across the fault plane (see Chap. 12, Tagami 2018).

10.1.4 FT Thermochronology as a Correlation Tool for Mesoscale Structural Data

In tectonically complex areas, the analysis of post-metamorphic deformation is particularly challenging, because deformation is often partitioned within different crustal blocks, fault orientation is not scale invariant, and the strain field inferred from mesoscale structures (i.e., outcrop scale) may differ from strain on a regional scale (Eyal and Reches 1983; Rebai et al. 1992; Martinez-Diaz 2002). Regional reconstructions thus require structural analysis at different scales, including field mapping of the network of major (km-scale) faults, and a dense distribution of time-constrained mesoscale strain axes that are derived from the kinematic analysis of fault-slip data in outcrops from high-strain and low-strain domains (Marrett and Allmendinger 1990). Within this framework, low-temperature thermochronology provides not only time constraints for the analysis of major faults, but also an effective tool to constrain the age of mesoscale deformation (e.g., Malusà et al. 2009a).

Fault-rock types and related deformation mechanisms show a generalised progression with depth (Fig. 10.4a); from gouge/breccias to cataclasites to mylonites, or to describe the mechanisms, from frictional-plastic to viscous flow (Sibson 1983; Snoke et al. 1998). The transition from frictional to viscous flow partly depends on strain rate, but it is dominantly controlled by lithology and temperature in the crust (Schmid and Handy 1991; Scholz 1998; Raterron et al. 2004). Therefore, the analysis of fault rocks in a specific lithology gives indications on the crustal level where mesoscale structures have formed. Because FT analysis provides chronological constraints on the passage of a rock through a given crustal level, the timing of both mesoscale structures and their associated strain axes can thus be constrained.

Crustal rocks are commonly dominated by quartz rheology; thus, the transition from frictional to viscous flow takes place at ~300 °C (Scholz 1998; Chen et al. 2013). The temperature of this change in deformational mechanism correlates well with the T_c of the FT system in low-damage zircon (Fig. 10.4a). Therefore, in general, mylonites will form at temperatures higher than the T_c of the zircon FT (ZFT) system. Cohesive cataclasites will form at temperatures that are higher than the T_c of the AFT system. Fault gouges and fault breccias are typical of the uppermost kilometres of the crust, i.e., of the temperature range best constrained by the AHe system (Fig. 10.4a). Because the frictional-to-viscous transition controls the thickness of the seismogenic zone (Priestley et al. 2008; Chen et al. 2013), the maximum depth extent for pseudotachylite formation in quartz-dominated crustal rocks also correlates with the T_c of

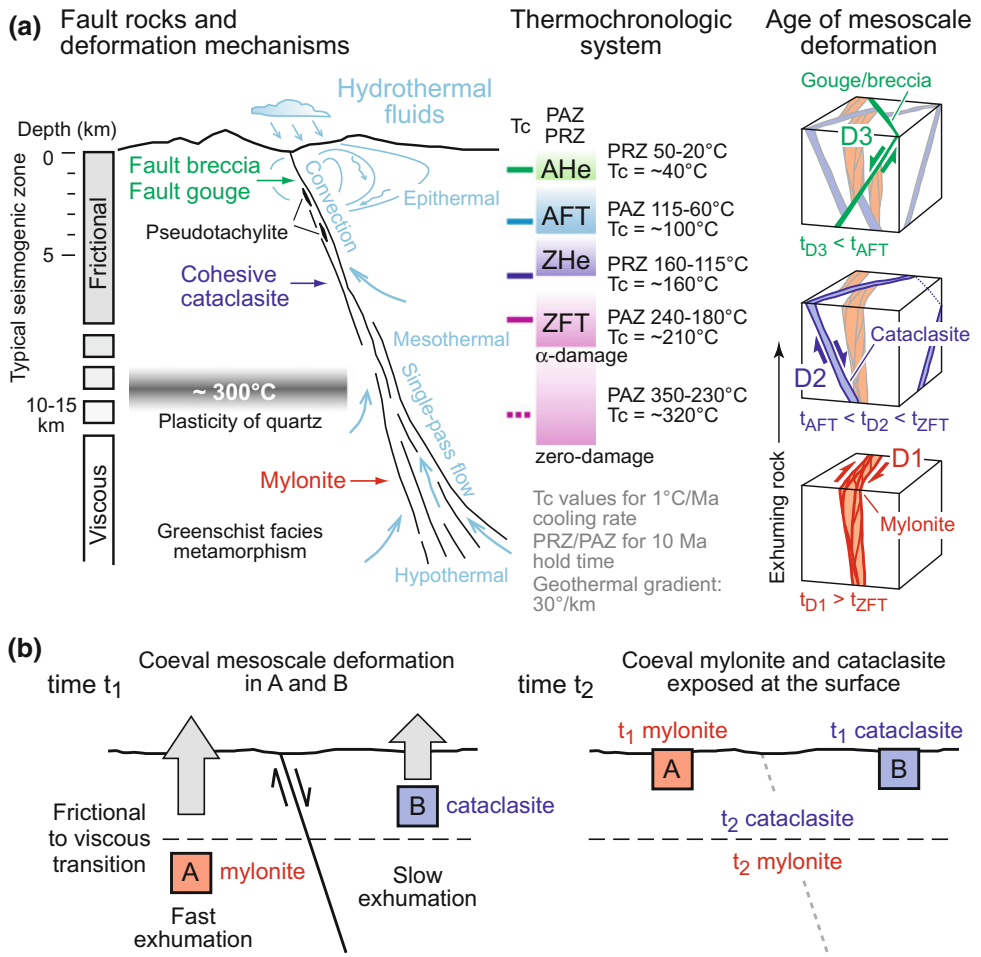

Fig. 10.4 **a** Fault-rock types and related deformation mechanisms show a generalised progression with depth. Mylonites in crustal rocks dominated by quartz rheology generally form at temperatures that are higher than the T_c of the ZFT system. Cohesive cataclasites generally form at temperatures that are higher than the T_c of the AFT system. Fault gouges and fault breccias are typical of the uppermost kilometres of the crust, i.e., of the temperature range best constrained by the AHe system. The panel on the right (3 cubes) conceptually illustrates the application of FT thermochronology to constrain the age of mesoscale deformation (and related strain axes) in a region where the exhumation history is independently constrained by AFT and ZFT data. During progressive exhumation, the rock mass is cut by a right-lateral shear zone marked by mylonitic rocks (phase D1), then by a normal fault marked by cohesive cataclasite (phase D2), and finally by a normal fault marked by gouge (phase D3). Phase D1 is probably older than the ZFT age, phase D2 may have taken place within a time range delimited by AFT and ZFT ages, whereas phase D3 is probably younger than the age provided by AFT (based on Malusà et al. 2009a). **b** Mylonites formed at time t_1 in rock mass A are now exposed at the surface (time t_2) adjacent to cataclasites (rock mass B). Both the mylonites and cataclasites formed at the same time but rock mass B formed at shallower levels, and was exhumed at slower rates. This example shows that fault-rock types alone cannot be used as a correlation tool for mesoscale structural data across different crustal blocks, because coeval deformation at the outcrop scale may be marked by different types of fault rocks. Integration with low-temperature thermochronology data is thus required for a correct interpretation of mesoscale structural data

the ZFT system (Fig. 10.4a). Fault rocks are often associated with veins and hydrothermal mineralisation that can provide additional constraints on the temperature of fault-rock formation (Wiltschko 1998).

Figure 10.4a conceptually illustrates the application of FT thermochronology to constrain the timing of mesoscale deformation and related strain axes, in a region where the exhumation history is independently constrained by AFT and ZFT ages. The rock mass (shown as a cube) in the right panel, during progressive exhumation is cut by a right-lateral shear zone marked by mylonitic rocks (phase D1), then by a normal fault marked by cohesive cataclasite (phase D2), and finally by a normal fault marked by gouge (phase D3). When combined with FT data, we can conclude that phase D1 is likely older than the ZFT age, phase D2 may have taken place within a time range delimited by AFT and ZFT ages, whereas deformation phase D3 is likely younger than the AFT age. If pseudotachylites are found along these faults,

they must be coeval or younger than the age provided by ZFT. The resolution of these constraints can be improved by using additional thermochronologic systems, and by considering not only rock types controlled by quartz rheology, but also other rock types controlled by the rheology of calcite, feldspar or olivine.

Interpreting mesoscale deformation on a regional scale solely based on deformation style, and without reliable time constraints provided by thermochronology, is potentially misleading. Deformation at the outcrop scale may be coeval in different crustal blocks, yet marked by different types of fault rock. Such a scenario may be possible if deformation occurred at the same time in different crustal blocks, but at different crustal levels (Malusà et al. 2009a). In the example of Fig. 10.4b, mylonites formed at time t_1 in one crustal block, are exposed at the surface together with cataclasites formed at the same time, but at shallower levels, in a nearby crustal block exhumed at slower rates. Therefore, deformation style should not be used for correlations of mesoscale structural data over large areas, unless integrated with low-temperature thermochronology data. The sampling strategy for this kind of study, that incorporates thermochronology and structural analysis, is similar to that required for the multiple-method approach (cf. Sect. 10.1.1). Samples should preferably be collected far enough away from major faults to avoid major perturbations of the background thermal field. Compared to the direct, typically more precise dating of synkinematic minerals grown along a fault plane (e.g., Freeman et al. 1997; Zwingmann and Mancktelow 2004), this approach generally requires a lower number of samples but does require multiple methods. However, it may provide constraints not only on single deformation steps, but on the whole deformation history recorded by sets of mesoscale faults.

10.2 Detrital Thermochronology Studies

Modern sediments and sedimentary rocks can provide invaluable information on the provenance and exhumation of the sediment sources (e.g., Baldwin et al. 1986; Cerveny et al. 1988; Brandon et al. 1998; Garver et al. 1999; Bernet et al. 2001; Willett et al. 2003; Ruiz et al. 2004; van der Beek et al. 2006). Sedimentary rocks for detrital thermochronology studies are typically collected through a stratigraphic succession. If sedimentary rocks have remained above the PAZ or partial retention zone (PRZ) of the chosen thermochronologic system since their deposition, the stratigraphic succession should reflect, in inverted order, the thermochronologic age structure observed in the sediment source area. Eroded detritus is generally distributed over a much wider area compared to that of the eroding source. Sedimentary successions thus record the erosional history of a much thicker crustal section. Today, such crustal sections may be completely eroded away, and thus impossible to investigate by the bedrock approach.

Detrital grain-age distributions represent the source rocks. Depending on the geologic evolution of the source rocks, these distributions can be unimodal or polymodal. Polymodal distributions are usually deconvolved into different grain-age populations (e.g., Brandon 1996; Dunkl and Székely 2002; Vermeesch 2009), which are generally older than the depositional age of the analysed sample (Bernet et al. 2004a; Bernet and Garver 2005).

10.2.1 Approaches to Detrital Thermochronology Studies

Figure 10.5a provides a summary of potential approaches to detrital thermochronology studies by using either modern sediment samples (1 and 2 in Fig. 10.5a) and samples from a stratigraphic succession (3–5 in Fig. 10.5a). Detrital thermochronology can provide information on:

Average long-term erosion rates (1 in Fig. 10.5a) Analysing minerals from samples of modern river sediments allows one to construct grain-age distributions from each catchment sampled (e.g., Garver et al. 1999; Brewer et al. 2003). These grain-age distributions are representative, under certain conditions, of the FT stratigraphy within the drainage (e.g., Bernet et al. 2004a; Resentini and Malusà 2012). The age of the youngest detrital age component, if interpreted as an exhumation-related cooling age, can be used to provide preliminary, although sometimes imprecise constraints on the average long-term (10^6–10^8 yr) erosion rate of the source area, using the lag-time approach (Garver et al. 1999) and a zero stratigraphic age (see below). Notably, grain-age distributions are influenced by the drainage hypsometry. Ages will be generally older in grains eroded from summits, and younger in grains eroded from valleys, depending on the age-elevation relationship in bedrock. In the case of well-developed age-elevation relationships, it is hypothetically possible to constrain the elevation from where sediment grains were eroded (e.g., Stock et al. 2006; Vermeesch 2007). Grain-age distributions will also vary depending on the mineral fertility of different upstream eroding lithologies. The mineral fertility, which can be defined as the variable propensity of different parent rocks to yield detrital grains of specific minerals when exposed to erosion (Moecher and Samson 2006; Malusà et al. 2016), can be quite inhomogeneous. The main advantage of using the detrital approach to constrain an average long-term erosion rate is the possibility of getting a first-order picture of the erosion pattern over large areas by using a relatively low number of samples (e.g., Bernet et al. 2004a; Malusà and Balestrieri 2012; Asti et al. 2018). However, ages related

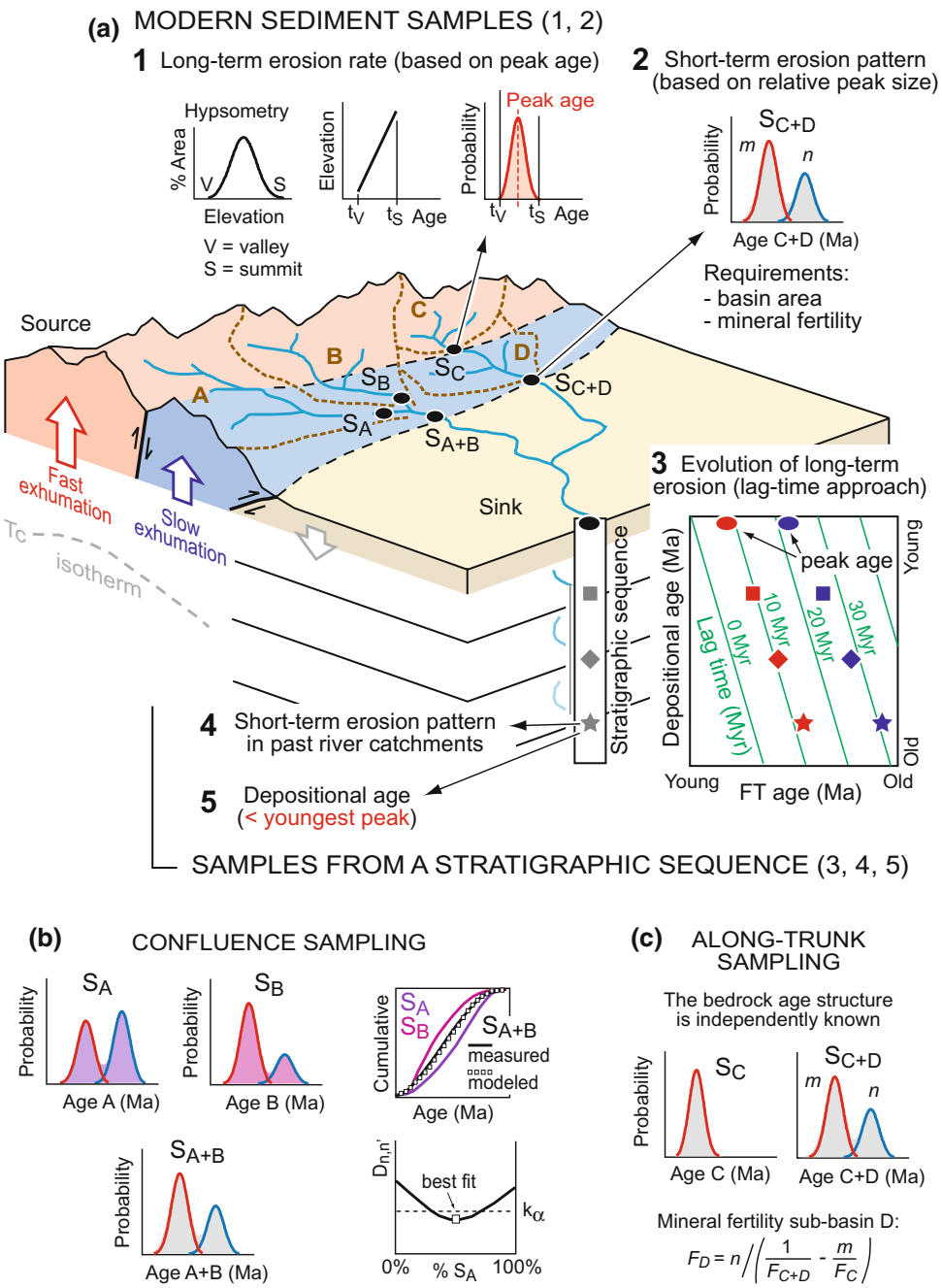

Fig. 10.5 Detrital thermochronologic analysis. **a** Cartoon showing the range of potential approaches and information retrieved from the thermochronologic analysis of modern sediment (1, 2) and sedimentary rocks (3, 4, 5); letters indicate sub-basins (A to D), hypothetical sampling sites (S) and relative peak size (*m*, *n*). Each approach is based on a range of assumptions that should be independently tested (see Table 10.1). Reliable constraints are best provided by integrating thermochronologic analysis of modern sediments, ancient sedimentary successions and independent mineral fertility determinations. **b**, **c** Alternative sampling strategies to perform sediment budgets based on the thermochronologic analysis of modern sediment samples (after Malusà et al. 2016); $D_{n,n'}$ is the maximum distance between cumulative frequency curves, K_α is the critical value for a significance level α (see Chap. 7, Malusà and Garzanti 2018)

to exhumational cooling should be distinguished from cooling ages that are independent from exhumation, such as those provided by volcanic grains. These grains can be effectively detected by double-dating (see Chap. 5, Danišík 2018; Chap. 7, Malusà and Garzanti 2018), as shown in Chap. 15 (Bernet 2018).

Modern short-term erosion patterns (2 in Fig. 10.5a) Grain-age distributions in modern river sediments can be analysed to constrain sediment budgets and erosion patterns on timescales typical of bedload river transport (generally 10^3–10^5 yr). This approach exploits the size of grain-age populations rather than the age of mineral grains, which is utilised instead as a provenance marker (Garver et al. 1999; Bernet et al. 2004b; Malusà et al. 2009b). Samples are either collected along the trunk of the river or at major confluences, and grain-age distributions are compared by statistical methods in order to determine the percentage of mineral grains derived from different sub-basins (see Sect. 10.2.2). This percentage, when integrated with the area of each sub-basin and its mineral fertility, which is independently derived (see Chap. 7, Malusà and Garzanti 2018), can be used to calculate the relative erosion rates of the sub-basins

(Malusà et al. 2016; 2017; Glotzbach et al. 2017, Braun et al. 2018). Relative erosion rates can be converted into absolute rates after integration with gauging data or cosmogenic-derived sediment fluxes for selected basins (e.g., Lupker et al. 2012; Wittmann et al. 2016). The same approach can be ideally applied to ancient alluvial sediments, using samples from lithified clastic sequences, whenever it can be reasonably assumed that the past mountain catchment was not markedly different from its present-day configuration (4 in Fig. 10.5a).

Evolution of long-term erosion rates (3 in Fig. 10.5a) The same approach utilised to constrain the average long-term erosion rate within a catchment (1 in Fig. 10.5a) can be extrapolated to ancient sedimentary successions to investigate the evolution of long-term erosion (10^6–10^8 yr timescales) in an adjacent orogen (e.g., Garver et al. 1999; Bernet et al. 2001; van der Beek et al. 2006). Samples are collected through a stratigraphic succession, and single minerals are analysed. The resulting grain-age distributions, when polymodal, are deconvolved into different grain-age populations (red and blue in Fig. 10.5), and these populations are then plotted on a lag-time diagram where the lag time is the difference between the cooling age and the depositional age (Garver et al. 1999), which is independently derived (e.g., by biostratigraphy or magnetostratigraphy). The lag time provides an estimate of the average exhumation rate of the analysed detrital grains from the depth of the T_c isothermal surface to the Earth's surface (Garver et al. 1999; Ruiz et al. 2004). The lag-time trend is often used to infer whether an eroding mountain belt is under a constructional, steady state or decay phase of evolution (Bernet et al. 2001; Carrapa et al. 2003; Spotila 2005; Ruiz and Seward 2006; Rahl et al. 2007; Zattin et al. 2010; Lang et al. 2016). More details and examples are provided in Chap. 15 (Bernet 2018) and Chap. 17 (Fitzgerald et al. 2018).

Depositional age (5 in Fig. 10.5a) Detrital thermochronology can be also used to constrain the depositional age of barren sedimentary successions (e.g., Carter et al. 1995; Rahn and Selbekk 2007). The depositional age of a sedimentary sample must be younger than the central age of the youngest grain-age population, provided that post-depositional annealing can be excluded.

10.2.2 Sediment Budgets Using Modern River Sediments

Constraining sediment budgets based on detrital thermochronology analysis of modern river sediments requires detrital sources with "thermochronologically distinct fingerprints". Such fingerprints are generally the result of different geologic or upper crustal exhumation histories (red and blue tectonic blocks in Fig. 10.5a). In a detrital sample exclusively derived from one of these sources (e.g., the fast exhuming red block sampled in catchment C), the grain-age distribution depends on the catchment hypsometry and on the catchment age-elevation relationship. Detrital samples derived from the mixing of various sources (e.g., samples S_{A+B} and S_{C+D}, Fig. 10.5a) likely yield polymodal grain-age distributions including different grain-age populations. Two alternative sampling strategies are employed for an effective partitioning of mineral grains (i.e., to determine the relative proportion of grains from each source), and to perform a sediment budget starting from the analysis of grain-age distributions. These are the confluence sampling and the along-trunk sampling approaches (Malusà et al. 2016).

Confluence sampling approach This requires collecting samples from major tributaries (S_A and S_B in Fig. 10.5a) and from the trunk river downstream of their confluence (S_{A+B} in Fig. 10.5a). Partitioning of detrital grains is based on a linear combination of grain-age distributions upstream of the confluence (e.g., Bernet et al. 2004b). The best-fit solution is defined by the mixing proportion that minimises the misfit between the modelled distributions resulting from the linear combination, and the empirical grain-age distribution observed downstream of the confluence (squares and black line, respectively, in the cumulative probability diagram in Fig. 10.5b). The goodness of fit between modelled and empirical grain-age distributions can be evaluated using the parameter $D_{n,n'}$ of the Kolmogorov–Smirnov statistics (Dunkl and Székely 2002; Malusà et al. 2013; Vermeesch 2013), which shows a minimum in correspondence of the best-fit solution. In order to avoid meaningless linear combinations between indistinguishable grain-age distributions, a two-sample Kolmogorov–Smirnov test can be used to check whether grain-age distributions in samples S_A and S_B are statistically different or not. The confluence sampling approach requires at least three samples at each node (S_A, S_B, and S_{A+B}). It allows a direct measurement of mineral fertility in sub-basins A and B using the same samples collected for thermochronologic analysis (see Chap. 7, Malusà and Garzanti 2018) and does not require any independent information on the thermochronologic fingerprint of the parent bedrock.

Along-trunk approach This approach can be used when a river cuts across rock units that have distinct, independently known thermochronologic signatures that do not overlap. Thus, the age populations can be used to unequivocally discriminate the provenance of detrital grains (Resentini and Malusà 2012). The relative proportion of grains from each source, according to the along-trunk approach is based on the deconvolution of grain-age distributions in individual age components of specific size (*m* and *n* in Fig. 10.5a, c) (e.g., Brandon 1996; Dunkl and Székely 2002). Only two samples (S_C and S_{C+D}) are needed for unmixing the thermochronologic signal and characterising

sub-basins C and D in terms of mineral fertility. Fertility of sub-basin C (F_C) is directly measured, fertility of sub-basin D (F_D) is calculated by the formula in Fig. 10.5c.

10.2.3 Assumptions in Detrital Thermochronology Studies

The approaches to detrital thermochronologic analysis illustrated in Fig. 10.5a rely on a range of assumptions that should be carefully considered and independently tested (see Table 10.1). When the age of a detrital population in a modern sediment sample is employed to constrain the long-term exhumation of bedrock exposed upstream of the sampling site (1 in Fig. 10.5a), the assumption is that the thermochronologic fingerprint of eroded bedrock reflects cooling during erosion. However, this assumption is not always valid. Thermochronologic ages may also reflect past transient changes in the thermal structure of the crust (Braun 2016), episodes of metamorphic or magmatic crystallisation within the eroded bedrock (Malusà et al. 2011; Kohn et al. 2015), or the cooling history of a different (distant) eroding source that provided detritus to sedimentary rocks now exposed within the drainage (Bernet and Garver 2005; von Eynatten and Dunkl 2012). Beside a careful evaluation of the geologic setting, the risk of misinterpretation can be minimised by multiple dating of detrital mineral grains (see Chap. 5, Danišík 2018), by the integration with thermochronologic analyses of cobbles (Chap. 17, Fitzgerald et al. 2018) and bedrock (Chap. 13, Baldwin et al. 2018), and by complementing detrital thermochronology analysis with thermal modelling (Ehlers et al. 2005; Braun et al. 2012).

The assumption of uniform mineral fertility in the catchment upstream of a sampling site, which is common to many detrital thermochronology studies (e.g., Glotzbach et al. 2013), should be carefully tested even in small basins, because grain ages sourced from elevation ranges characterised by low-fertility rocks would be under-represented in corresponding detrital grain-age distributions. This is particularly important when detrital and bedrock thermochronology data are compared to test if a mountain range is in steady state (e.g., Brewer et al. 2003; Ruhl and Hodges 2005). The analysis of the short-term erosion pattern based on the relative proportion of different grain-age populations in polymodal samples (2, Fig. 10.5a) relies on the additional assumption that the sediment is effectively mixed, and that the potential bias possibly introduced by hydraulic processes during sediment transport and deposition is negligible. These assumptions can be tested using the strategies described in Chap. 7 (Malusà and Garzanti 2018).

The number of often untestable assumptions underlying the detrital thermochronologic approach largely increases in ancient sedimentary successions (see Table 10.1 and references therein). Compared to approaches 1 and 2 in Fig. 10.5a, lag-time analysis (3 in Fig. 10.5a) additionally implies that: (i) the time elapsed during sediment transport is negligible; (ii) the isothermal surfaces relevant for the chosen thermochronologic system have remained steady during exhumation; (iii) major changes in provenance can be excluded or can be detected and accounted for; (iv) the thermochronologic signal is not modified by post-depositional annealing.

Apart from transport by turbidity currents, the zero transport time assumption from erosion to deposition should be evaluated on a case-by-case basis. As an example, the transportation of apatite and zircon as river bedload in the Amazon basin may require a few millions of years, as attested by cosmogenic data (Wittmann et al. 2011). Thus, transportation time may become relevant for lag-time interpretation. The behaviour of isothermal surfaces during exhumation is generally difficult to predict (see Chap. 8, Malusà and Fitzgerald 2018) and may require an integrated approach including thermochronologic data from the source region and thermal modelling. A reliable assessment of detritus provenance generally requires a multiple-method approach to single-grain analysis (see Chap. 5, Danišík 2018; Chap. 14, Carter 2018) and a careful inspection of thermochronologic age trends along a stratigraphic succession (see Chap. 16, Malusà 2018). Lag-time analysis of detrital mineral grains is often utilised to infer the long-term evolution of an entire mountain range, but it is noteworthy that it may emphasise the cooling history of small parts of the mountain range that are characterised by highest mineral fertility (Malusà et al. 2017). The potential impact of post-depositional annealing may represent a problem not only for lag-time analysis, but also for the determination of the depositional age of a sedimentary rock by thermochronologic methods (5 in Fig. 10.5a). However, post-depositional annealing produces age trends that can be recognised when multiple samples are analysed along a stratigraphic succession (van der Beek et al. 2006, see Chap. 16, Malusà 2018 and Chap. 17, Fitzgerald et al. 2018). In this perspective, information on burial-related annealing derived from AFT length distributions gives this method a further advantage over other thermochronology methods that rely on age values only.

Table 10.1 Main assumptions for different approaches to detrital thermochronology and potential impact on data interpretation

Assumption and approach (identified by number code)	Alternative scenarios	References	Potential impact on data interpretation	How to test	This book
Thermochronologic ages in detritus reflect cooling of eroded bedrock during erosional exhumation (*1*, **3**)	Ages may reflect transient changes in the thermal structure of the crust, episodes of metamorphic or magmatic crystallisation, or cooling of distant sediment sources	Bernet and Garver (2005), Malusà et al. (2011), Braun (2016)	*Major*: misinterpretation of cooling ages in terms of exhumation of eroded bedrock	Multiple dating of mineral grains; integration with analysis of cobbles and bedrock, and thermal modelling	Chaps. 5, 8 and 17
Sediment is effectively mixed, grain-age distributions are not affected by hydraulic sorting (*1*, *2*, **3**, **4**)	A relationship between grain age and grain size may imply a potential vulnerability of grain-age distributions to hydraulic processes	Bernet et al. (2004a), Malusà et al. (2013)	*Moderate*: under-representation of specific grain-age populations in detritus	Assessment of age-size relationships in detritus, detection of placer lags	Chap. 7
Mineral fertility does not vary within the river catchment upstream of the sampling site (*1*)	Bedrock shows variable mineral fertility depending on the elevation (grain ages associated to low-fertility rocks are under-represented in detritus)	Brewer et al. (2003), Malusà et al. (2016)	*Moderate to major*: biased reconstruction of catchment FT stratigraphy; flawed evaluation of steady-state conditions	Inspection of bedrock geology; measurement of mineral fertility	Chap. 7
Mineral fertility does not vary regionally in a mountain belt, units are represented in detritus according to their size and erosion rate (*2*, **3**)	Mineral fertility varies over orders of magnitude across a mountain belt, tectonic units with lower mineral fertility are under-represented in the detrital record	Dickinson (2008), Malusà et al. (2017)	*Major:* lag-time analysis only constrains the evolution of high-fertility tectonic units; sediment budgets are incorrect	Inspection of bedrock geology; measurement of mineral fertility	Chap. 7
Sediment transport time from the source rocks to the final sink is negligible (**3**)	Minerals grains transported as bedload (e.g., apatite and zircon) may take a few millions of years to reach their final sediment sink	Garver et al. (1999), Wittmann et al. (2011)	*Moderate*: underestimation of exhumation rates based on lag-time analysis	Comparison between magmatic-age peaks and stratigraphic age of analysed samples	Chaps. 7 and 16
T_c isotherms have remained steady during exhumation (**3**)	Isotherms move upward due to heat advection triggered by fast erosion, and are then restored after thermal relaxation	Rahl et al. (2007), Braun (2016)	*Major*: unreliable erosion rate estimations; ages may record thermal relaxation, not erosion	Integration with thermal modelling	Chap. 8
No provenance change, lag-time pertains to a single eroding source (**3**)	Major provenance changes are recorded along the stratigraphic sequence	Ruiz et al. (2004), Glotzbach et al. (2011)	*Major*: incorrect recognition of lag-time trends if provenance changes remain undetected	Multi-dating approach and integration with other provenance constraints	Chaps. 5, 14 and 16
The drainage network has remained steady through time, same mineral fertility in bedrock eroded in the past and in bedrock eroded today (**4**)	Major drainage reorganisation, different bedrock geology in paleo- and modern river catchments	Garzanti and Malusà (2008)	*Major*: the past short-term erosion pattern based on sediment budgets is incorrect	Geomorphologic analysis; independent provenance constraints	Chap. 14
The detrital thermochronologic signal is preserved after deposition (**3**, **5**)	The detrital thermochronologic signal is modified by post-depositional annealing	van der Beek et al. (2006), Chirouze et al. (2012)	*Major*: incorrect constraints to the maximum depositional age; overestimation of exhumation rates based on lag-time analysis	Careful inspection of age trends along the stratigraphic succession	Chaps. 16 and 17

1 Average long-term erosion rates; *2* Modern short-term erosion patterns; **3** Evolution of long-term erosion rates by the lag-time approach; **4** Past short-term erosion patterns; **5** Determination of depositional age (in italics, approaches based on the analysis of modern sediments; in bold, approaches based on the analysis of sedimentary rocks)

10.3 Conclusions

Low-temperature thermochronology can be used to constrain a range of geologic processes using bedrock and/or detrital samples. In bedrock studies, the multiple-method and age-elevation approaches provide useful constraints on the exhumation history of rocks now exposed at the surface, provided that a range of assumptions are properly evaluated. The multiple-method approach provides direct constraints on the cooling history of a sample, but the paleogeothermal gradient must be independently known to convert an average cooling rate to an average exhumation rate. The age-elevation approach does not require explicit assumptions on the paleogeothermal gradient. A careful analysis of the relationships between the topography and the thermal reference frame is anyway required, as is an understanding of the various factors that may change the slope of an age-elevation profile. Multiple methods can be applied to the same array of vertical profile samples, which allows exhumation to be constrained over longer time intervals. FT stratigraphy provides a suitable reference frame to constrain virtual configurations of eroded rock units above the present-day topography. A range of thermochronologic markers can be used to highlight episodes of differential exhumation across a major fault and constrain the timing of fault activity. However, in some cases, major episodes of faulting are not revealed by low-temperature thermochronology. FT data combined with the analysis of fault rocks also provide useful constraints on the timing of mesoscale deformation, and a reliable tool for the correlation over large areas of mesoscale strain axes derived from fault-slip analysis.

Detrital thermochronologic analysis can be used to provide an averaged image of the thermochronologic age structure in bedrock and to constrain the erosion pattern of the sediment sources on short-term (10^3–10^5 yr) and long-term (10^6–10^8 yr) timescales. Detrital thermochronologic analysis can also be used to constrain the provenance of the dated grains. The analysis of modern sediment samples provides the baseline for the thermochronologic interpretation of older stratigraphic levels. The lag-time approach to detrital thermochronology provides information that can be used to investigate the evolutionary stage of an entire orogenic belt, and infer whether it is under a constructional, steady state or decay phase of evolution. Different approaches to detrital thermocronology are based on a range of assumptions that should be independently tested to avoid meaningless geologic interpretations. Depending on the objectives, the full potential of the detrital thermochronologic approach is best exploited by the integrated analysis of samples collected along a sedimentary succession, samples of modern river sediment, and independent mineral fertility determinations.

Acknowledgements This work benefited from constructive reviews by Maria Laura Balestrieri and Shari Kelley, comments on an early version of the manuscript by an anonymous reviewer, and comments by Suzanne Baldwin and students in her 2016 thermochronology class. PGF thanks the National Science Foundation for funding through the years as well as support from Jarg Pettinga and the Erksine Program at the University of Canterbury.

References

Asti R, Malusà MG, Faccenna C (2018) Supradetachment basin evolution unraveled by detrital apatite fission track analysis: the Gediz Graben (Menderes Massif, Western Turkey). Basin Res 30:502-521

Baldwin SL, Harrison TM, Burke K (1986) Fission track evidence for the source of Scotland District sediments, Barbados and implications for post-Eocene tectonics of the southern Caribbean. Tectonics 5:457–468

Baldwin SL, Fitzgerald PG, Malusà MG (2018) Chapter 13. Crustal exhumation of plutonic and metamorphic rocks: constraints from fission-track thermochronology. In: Malusà MG, Fitzgerald PG (eds) Fission-track thermochronology and its application to geology. Springer, Berlin

Balestrieri ML, Bonini M, Corti G, Sani F, Philippon M (2016) A refinement of the chronology of rift-related faulting in the broadly rifted zone, southern Ethiopia, through apatite fission-track analysis. Tectonophysics 671:42–55

Bernet M (2018) Chapter 15. Exhumation studies of mountain belts based on detrital fission-track analysis on sand and sandstones. In: Malusà MG, Fitzgerald PG (eds) Fission-track thermochronology and its application to geology. Springer, Berlin

Bernet M, Garver JI (2005) Fission-track analysis of detrital zircon. Rev Mineral Geochem 58(1):205–237

Bernet M, Zattin M, Garver JI, Brandon MT, Vance JA (2001) Steady-state exhumation of the European Alps. Geology 29:35–38

Bernet M, Brandon MT, Garver JI, Molitor B (2004a) Fundamentals of detrital zircon fission-track analysis for provenance and exhumation studies with examples from the European Alps. Geol Soc Am Spec Pap 378:25–36

Bernet M, Brandon MT, Garver JI, Molitor B (2004b) Downstream changes of Alpine zircon fission-track ages in the Rhône and Rhine Rivers. J Sediment Res 74:82–94

Bernoulli D, Bertotti G, Zingg A (1989) Northward thrusting of the Gonfolite Lombarda (South-Alpine Molasse) onto the Mesozoic sequence of the Lombardian Alps: implications for the deformation history of the Southern Alps. Eclogae Geol Helv 82:841–856

Bigot-Cormier F, Poupeau G, Sosson M (2000) Differential denudations of the Argentera Alpine external crystalline massif (SE France) revealed by fission track thermochronology (zircons, apatites). C R Acad Sci 5:363–370

Brandon MT (1996) Probability density plot for fission-track grain-age samples. Radiat Meas 26:663–676

Brandon MT, Roden-Tice MK, Garver JI (1998) Late Cenozoic exhumation of the Cascadia accretionary wedge in the Olympic Mountains, northwest Washington State. Geol Soc Am Bull 110:985–1009

Braun J (2002) Quantifying the effect of recent relief changes on age–elevation relationships. Earth Planet Sci Lett 200(3):331–343

Braun J (2016) Strong imprint of past orogenic events on the thermochronological record. Tectonophysics 683:325–332

Braun J, Gemignani L, van der Beek P (2018) Extracting information on the spatial variability in erosion rate stored in detrital cooling age distributions in river sands. Earth Surf Dynam 6:257–270

Braun J, van der Beek P, Valla P, Robert X, Herman F, Glotzbach C, Pedersen V, Perry C, Simon-Labric T (2012) Quantifying rates of landscape evolution and tectonic processes by thermochronology and numerical modeling of crustal heat transport using PECUBE. Tectonophysics 524–525:1–28

Brewer ID, Burbank DW, Hodges KV (2003) Modelling detrital cooling-age populations: insights from two Himalayan catchments. Basin Res 15:305–320

Brown RW (1991) Backstacking apatite fission-track "stratigraphy": a method for resolving the erosional and isostatic rebound components of tectonic uplift histories. Geology 19(1):74–77

Brown RW, Summerfield MA, Gleadow AJW (1994) Apatite fission track analysis: its potential for the estimation of denudation rates and implications of long-term landscape development. In: Kirkby MJ (ed) Process models and theoretical geomorphology. Wiley, Hoboken, pp 23–53

Carrapa B, Wijbrans J, Bertotti G (2003) Episodic exhumation in the Western Alps. Geology 31(7):601–604

Carter A (2018) Chapter 14. Thermochronology on sand and sandstones for stratigraphic and provenance studies. In: Malusà MG, Fitzgerald PG (eds) Fission-track thermochronology and its application to geology. Springer, Berlin

Carter A, Bristow CS, Hurford AJ (1995) The application of fission track analysis to the dating of barren sequences: examples from red beds in Scotland and Thailand. Geol Soc Spec Publ 89:57–68

Cerveny PF, Naeser ND, Zeitler PK, Naeser CW, Johnson NM (1988) History of uplift and relief of the Himalaya during the past 18 million years: evidence from fission-track ages of detrital zircons from sandstones of the Siwalik Group. New perspectives in basin analysis. Springer, New York, pp 43–61

Chen WP, Yu CQ, Tseng TL, Yang Z, Wang CY, Ning J, Leonard T (2013) Moho, seismogenesis, and rheology of the lithosphere. Tectonophysics 609:491–503

Chirouze F, Bernet M, Huyghe P, Erens V, Dupont-Nivet G, Senebier F (2012) Detrital thermochronology and sediment petrology of the middle Siwaliks along the Muksar Khola section in eastern Nepal. J Asian Earth Sci 44:94–106

D'Adda P, Zanchi A, Bergomi M, Berra F, Malusà MG, Tunesi A, Zanchetta S (2011) Polyphase thrusting and dyke emplacement in the central Southern Alps (northern Italy). Int J Earth Sci 100:1095–1113

Danišík M (2018) Chapter 5. Integration of fission-track thermochronology with other geochronologic methods on single crystals. In: Malusà MG, Fitzgerald PG (eds) Fission-track thermochronology and its application to geology. Springer, Berlin

Dickinson WR (2008) Impact of differential zircon fertility of granitoid basement rocks in North America on age populations of detrital zircons and implications for granite petrogenesis. Earth Planet Sci Lett 275:80–92

Dunkl I, Székely B (2002) Component analysis with visualization of fitting—PopShare, a windows program for data analysis. Goldschmidt conference abstracts 2002. Geochim Cosmochim Ac 66/A:201

Ehlers TA (2005) Crustal thermal processes and the interpretation of thermochronometer data. Rev Mineral Geochem 58:315–350

Ehlers TA, Chaudhri T, Kumar S, Fuller CW, Willett SD, Ketcham RA, Brandon MT, Belton DX, Kohn BP, Gleadow AJW, Dunai TJ, Fu FQ (2005) Computational tools for low-temperature thermochronometer interpretation. Rev Mineral Geochem 58(1):589–622

Eyal Y, Reches Z (1983) Tectonic analysis of the Dead Sea Rift region since the Late-Cretaceous based on mesostructures. Tectonics 2:167–185

Feinstein S, Kohn B, Osadetz K, Price RA (2007) Thermochronometric reconstruction of the prethrust paleogeothermal gradient and initial thickness of the Lewis thrust sheet, southeastern Canadian Cordillera foreland belt. Geol Soc Am Spec Pap 433:167–182

Fitzgerald PG (1992) The Transantarctic Mountains of southern Victoria Land: the application of apatite fission track analysis to a rift shoulder uplift. Tectonics 11(3):634–662

Fitzgerald PG (1994) Thermochronologic constraints on post-Paleozoic tectonic evolution of the central Transantarctic Mountains, Antarctica. Tectonics 13:818–836

Fitzgerald PG, Gleadow AJ (1988) Fission-track geochronology, tectonics and structure of the Transantarctic Mountains in northern Victoria Land, Antarctica. Chem Geol 73(2):169–198

Fitzgerald PG, Gleadow AJ (1990) New approaches in fission track geochronology as a tectonic tool: examples from the Transantarctic Mountains. Int J Rad Appl Instr Part D Nucl Tracks Rad Meas 17 (3):351–357

Fitzgerald PG, Malusà MG (2018) Chapter 9. Concept of the exhumed partial annealing (retention) zone and age-elevation profiles in thermochronology. In: Malusà MG, Fitzgerald PG (eds) Fission-track thermochronology and its application to geology. Springer, Berlin

Fitzgerald PG, Sorkhabi RB, Redfield TF, Stump E (1995) Uplift and denudation of the central Alaska Range: a case study in the use of apatite fission track thermochronology to determine absolute uplift parameters. J Geophys Res Sol Earth 100(B10):20175–20191

Fitzgerald PG, Duebendorfer EM, Faulds JE, O'Sullivan PB (2009) South Virgin–White Hills detachment fault system of SE Nevada and NW Arizona: applying apatite fission track thermochronology to constrain the tectonic evolution of a major continental detachment fault. Tectonics 28

Fitzgerald PG, Malusà MG, Muñoz JA (2018) Chapter 17. Detrital thermochronology using conglomerates and cobbles. In: Malusà MG, Fitzgerald PG (eds) Fission-track thermochronology and its application to geology. Springer, Berlin

Foster DA (2018) Chapter 11. Fission-track thermochronology in structural geology and tectonic studies. In: Malusà MG, Fitzgerald PG (eds) Fission-track thermochronology and its application to geology. Springer, Berlin

Foster DA, Gleadow AJW (1996) Structural framework and denudation history of the flanks Kenya and Anza rifts, East Africa. Tectonics 15:258–271

Foster DA, Gleadow AJ, Reynolds SJ, Fitzgerald PG (1993) Denudation of metamorphic core complexes and the reconstruction of the transition zone, west central Arizona: constraints from apatite fission track thermochronology. J Geophys Res Sol Earth 98 (B2):2167–2185

Freeman SR, Inger S, Butler RWH, Cliff RA (1997) Dating deformation using Rb–Sr in white mica: greenschist facies deformation ages from the Entrelor shear zone, Italian Alps. Tectonics 16:57–76

Gallagher K, Brown RW (1997) The onshore record of passive margin evolution. J Geol Soc Lond 154:451–457

Garver JI, Brandon MT, Roden-Tice MK, Kamp PJJ (1999) Exhumation history of orogenic highlands determined by detrital fission track thermochronology. Geol Soc Spec Publ 154:283–304

Garzanti E, Malusà MG (2008) The Oligocene Alps: domal unroofing and drainage development during early orogenic growth. Earth Planet Sci Lett 268:487–500

Gessner K, Ring U, Johnson C, Hetzel R, Passchier CW, Güngör T (2001) An active bivergent rolling-hinge detachment system: Central Menderes metamorphic core complex in western Turkey. Geology 29:611–614

Gleadow AJW, Fitzgerald PG (1987) Uplift history and structure of the Transantarctic Mountains: new evidence from fission track dating of

basement apatites in the Dry Valleys area, southern Victoria Land. Earth Planet Sci Lett 82(1):1–14
Glotzbach C, Bernet M, van der Beek P (2011) Detrital thermochronology records changing source areas and steady exhumation in the Western European Alps. Geology 39(3):239–242
Glotzbach C, van der Beek P, Carcaillet J, Delunel R (2013) Deciphering the driving forces of erosion rates on millennial to million-year timescales in glacially impacted landscapes: an example from the Western Alps. J Geophys Res Earth 118:1491–1515
Glotzbach C, Busschers FS, Winsemann J (2017) Detrital thermochronology of Rhine, Elbe and Meuse river sediment (Central Europe): implications for provenance, erosion and mineral fertility. Int J Earth Sci. https://doi.org/10.1007/s00531-017-1502-9
Green PF (1986) On the thermo-tectonic evolution of Northern England: evidence from fission track analysis. Geol Mag 153:493–506
Green PF, Duddy IR, Laslett GM, Hegarty KA, Gleadow AJW, Lovering JF (1989) Thermal annealing of fission tracks in apatite 4. Quantitative modelling techniques and extension to geological timescales. Chem Geol Isot Geosci Sect 79(2):155–182
Hendriks B, Andriessen P, Huigen Y, Leighton C, Redfield T, Murrell G, Gallagher K, Nielsen SB (2007) A fission track data compilation for Fennoscandia. Norw J Geol 87:143–155
Herman F, Braun J, Dunlap WJ (2007) Tectonomorphic scenarios in the Southern alps of New Zealand. J Geophys Res Sol Earth 112 (B4)
Hurford AJ (1986) Cooling and uplift patterns in the Lepontine Alps South Central Switzerland and an age of vertical movement on the insubric fault line. Contrib Miner Petrol 92:413–427
Ketcham R (2018) Chapter 3. Fission track annealing: from geologic observations to thermal history modeling. In: Malusà MG, Fitzgerald PG (eds) Fission-track thermochronology and its application to geology. Springer, Berlin
Kohn MJ, Corrie SL, Markley C (2015) The fall and rise of metamorphic zircon. Am Miner 100(4):897–908
Kounov A, Viola G, De Wit M, Andreoli MAG (2009) Denudation along the Atlantic passive margin: new insights from apatite fission-track analysis on the western coast of South Africa. Geol Soc Spec Publ 324:287–306
Ksienzyk AK, Dunkl I, Jacobs J, Fossen H, Kohlmann F (2014) From orogen to passive margin: constraints from fission track and (U–Th)/He analyses on Mesozoic uplift and fault reactivation in SW Norway. Geol Soc Spec Publ 390
Labaume P, Jolivet M, Souquière F, Chauvet A (2008) Tectonic control on diagenesis in a foreland basin: combined petrologic and thermochronologic approaches in the Grès d'Annot basin (Late Eocene-Early Oligocene, French-Italian external Alps). Terra Nova 20:95–101
Lang KA, Huntington KW, Burmester R, Housen B (2016) Rapid exhumation of the eastern Himalayan syntaxis since the late Miocene. Geol Soc Am Bull 128:1403–1422
Lupker M, Blard PH, Lavé J, France-Lanord C, Leanni L, Puchol N, Charreau J, Bourlès D (2012) ^{10}Be-derived Himalayan denudation rates and sediment budgets in the Ganga basin. Earth Planet Sci Lett 333:146–156
Malusà MG (2018) Chapter 16. A guide for interpreting complex detrital age patterns in stratigraphic sequences. In: Malusà MG, Fitzgerald PG (eds) Fission-track thermochronology and its application to geology. Springer, Berlin
Malusà MG, Balestrieri ML (2012) Burial and exhumation across the Alps-Apennines junction zone constrained by fission-track analysis on modern river sands. Terra Nova 24:221–226
Malusà MG, Fitzgerald PG (2018) Chapter 8. From cooling to exhumation: setting the reference frame for the interpretation of thermocronologic data. In: Malusà MG, Fitzgerald PG (eds) Fission-track thermochronology and its application to geology. Springer, Berlin
Malusà MG, Garzanti E (2018) Chapter 7. The sedimentology of detrital thermochronology. In: Malusà MG, Fitzgerald PG (eds) Fission-track thermochronology and its application to geology. Springer, Berlin
Malusà MG, Polino R, Zattin M, Bigazzi G, Martin S, Piana F (2005) Miocene to present differential exhumation in the Western Alps: insights from fission track thermochronology. Tectonics 24(3): TC3004:1-23
Malusà MG, Philippot P, Zattin M, Martin S (2006) Late stages of exhumation constrained by structural, fluid inclusion and fission track analyses (Sesia–Lanzo unit, Western European Alps). Earth Planet Sci Lett 243(3):565–580
Malusà MG, Polino R, Cerrina Feroni A, Ellero A, Ottria G, Baidder L, Musumeci G (2007) Post-Variscan tectonics in eastern Anti-Atlas (Morocco). Terra Nova 19(6):481–489
Malusà MG, Polino R, Zattin M (2009a) Strain partitioning in the axial NW Alps since the Oligocene. Tectonics 28(TC002370):1–26
Malusà MG, Zattin M, Andò S, Garzanti E, Vezzoli G (2009b) Focused erosion in the Alps constrained by fission-track ages on detrital apatites. Geol Soc Spec Publ 324:141–152
Malusà MG, Villa IM, Vezzoli G, Garzanti E (2011) Detrital geochronology of unroofing magmatic complexes and the slow erosion of Oligocene volcanoes in the Alps. Earth Planet Sci Lett 301:324–336
Malusà MG, Carter A, Limoncelli M, Villa IM, Garzanti E (2013) Bias in detrital zircon geochronology and thermochronometry. Chem Geol 359:90–107
Malusà MG, Resentini A, Garzanti E (2016) Hydraulic sorting and mineral fertility bias in detrital geochronology. Gondwana Res 31:1–19
Malusà MG, Wang J, Garzanti E, Liu ZC, Villa IM, Wittmann H (2017) Trace-element and Nd-isotope systematics in detrital apatite of the Po river catchment: implications for provenance discrimination and the lag-time approach to detrital thermochronology. Lithos 290–291:48–59
Mancktelow NS, Grasemann B (1997) Time-dependent effects of heat advection and topography on cooling histories during erosion. Tectonophysics 270(3):167–195
Marrett R, Allmendinger RW (1990) Kinematic analysis of fault-slip data. J Struct Geol 12:973–986
Martinez-Diaz JJ (2002) Stress field variation related to fault interaction in a reverse oblique-slip fault: the Alhama de Murcia fault, Betic Cordillera, Spain. Tectonophysics 356:291–305
Miller SR, Fitzgerald PG, Baldwin SL (2010) Cenozoic range-front faulting and development of the Transantarctic Mountains near Cape Surprise, Antarctica: thermochronologic and geomorphologic constraints. Tectonics 29(1)
Moecher DP, Samson SD (2006) Differential zircon fertility of source terranes and natural bias in the detrital zircon record: implications for sedimentary provenance analysis. Earth Planet Sci Lett 247:252–266
Moore MA, England PC (2001) On the inference of denudation rates from cooling ages of minerals. Earth Planet Sci Lett 185:265–284
Murakami M, Tagami T (2004) Dating pseudotachylyte of the Nojima fault using the zircon fission-track method. Geophys Res Lett 31(12)
Naeser CW, Bryant B, Crittenden MD, Sorensen ML (1983) Fission-track ages of apatite in the Wasatch Mountains, Utah: an uplift study. Geol Soc Am Mem 157:29–36
Niemi NA, Buscher JT, Spotila JA, House MA, Kelley SA (2013) Insights from low-temperature thermochronometry into transpressional deformation and crustal exhumation along the San Andreas fault in the western Transverse Ranges, California. Tectonics 32:1602–1622

Oberli F, Meier M, Berger A, Rosenberg CL, Gieré R (2004) U–Th–Pb and 230Th/238U disequilibrium isotope systematics: precise accessory mineral chronology and melt evolution tracing in the Alpine Bergell intrusion. Geochim Cosmochim Acta 68:2543–2560

Pieri M, Groppi G (1981) Subsurface geological structure of the Po Plain, Italy. Progetto Finalizzato Geodinamica 414:1–13

Priestley K, Jackson J, McKenzie D (2008) Lithospheric structure and deep earthquakes beneath India, the Himalaya and southern Tibet. Geophys J Int 172:345–362

Raab MJ, Brown RW, Gallagher K, Carter A, Weber K (2002) Late Cretaceous reactivation of major crustal shear zones in northern Namibia: constraints from apatite fission track analysis. Tectonophysics 349:75–92

Rahl JM, Ehlers TA, van der Pluijm BA (2007) Quantifying transient erosion of orogens with detrital thermochronology from syntectonic basin deposits. Earth Planet Sci Lett 256:147–161

Rahn MK, Selbekk R (2007) Absolute dating of the youngest sediments of the Swiss Molasse basin by apatite fission track analysis. Swiss J Geosci 100(3):371–381

Raterron P, Wu Y, Weidner DJ, Chen J (2004) Low-temperature olivine rheology at high pressure. Phys Earth Planet Inter 145:149–159

Rebai S, Philip H, Taboada A (1992) Modern tectonic stress field in the Mediterranean region: evidence for variations in stress directions at different scales. Geophys J Int 110:106–140

Reiners PW, Brandon MT (2006) Using thermochronology to understand orogenic erosion. Annu Rev Earth Planet Sci 34:419–466

Resentini A, Malusà MG (2012) Sediment budgets by detrital apatite fission-track dating (Rivers Dora Baltea and Arc, Western Alps). Geol Soc Am Spec Pap 487:125–140

Riccio SJ, Fitzgerald PG, Benowitz JA, Roeske SM (2014) The role of thrust faulting in the formation of the eastern Alaska Range: thermochronological constraints from the Susitna glacier thrust fault region of the intracontinental strike-slip Denali fault system. Tectonics 33(11):2195–2217

Richardson NJ, Densmore AL, Seward D et al (2008) Extraordinary denudation in the Sichuan basin: insights from low-temperature thermochronology adjacent to the eastern margin of the Tibetan Plateau. J Geophys Res Solid Earth 113(B4)

Ruhl KW, Hodges KV (2005) The use of detrital mineral cooling ages to evaluate steady state assumptions in active orogens: an example from the central Nepalese Himalaya. Tectonics 24

Ruiz G, Seward D (2006) The Punjab foreland basin of Pakistan: a reinterpretation of zircon fission-track data in the light of Miocene hinterland dynamics. Terra Nova 18:248–256

Ruiz G, Seward D, Winkler W (2004) Detrital thermochronology—a new perspective on hinterland tectonics, an example from the Andean Amazon Basin, Ecuador. Basin Res 16:413–430

Ruiz G, Carlotto V, Van Heiningen PV, Andriessen PAM (2009) Steady-state exhumation pattern in the Central Andes–SE Peru. Geol Soc Spec Publ 324:307–316

Schildgen TF, van der Beek PA (2018) Chapter 19. Application of low-temperature thermochronology to the geomorphology of orogenic systems. In: Malusà MG, Fitzgerald PG (eds) Fission-track thermochronology and its application to geology. Springer, Berlin

Schmid SM, Handy MR (1991) Towards a genetic classification of fault rocks: geological usage and tectonophysical implications. In: Muller DW et al (eds) Controversies in modern geology. Academic Press, Cambridge, pp 339–361

Schneider DA, Issler DR (2018) Chapter 18. Application of low-temperature thermochronology to hydrocarbon exploration. In: Malusà MG, Fitzgerald PG (eds) Fission-track thermochronology and its application to geology. Springer, Berlin

Scholz CH (1998) Earthquakes and friction laws. Nature 391:37–42

Schwartz S, Gautheron C, Audin L, Dumont T, Nomade J, Barbarand J, Pinna-Jamme R, van der Beek P (2017) Foreland exhumation controlled by crustal thickening in the Western Alps. Geology G38561-1

Sibson RH (1983) Continental fault structure and the shallow earthquake source. J Geol Soc Lond 140:741–767

Snoke AW, Tullis J, Todd VR (1998) Fault-related rocks: a photographic atlas. Princeton University Press, Princeton

Spotila JA (2005) Applications of low-temperature thermochronometry to quantification of recent exhumation in mountain belts. Rev Miner Geochem 58(1):449–466

Stock GM, Ehlers TA, Farley KA (2006) Where does sediment come from? Quantifying catchment erosion with detrital apatite (U–Th)/He thermochronometry. Geology 34:725–728

Stockli DF, Surpless BE, Dumitru TA, Farley KA (2002) Thermochronological constraints on the timing and magnitude of Miocene and Pliocene extension in the central Wassuk Range, western Nevada. Tectonics 21

Stüwe K, White L, Brown R (1994) The influence of eroding topography on steady-state isotherms. Application to fission-track analysis. Earth Planet Sci Lett 124(1–4):63–74

Tagami T. (2018) Chapter 12. Application of fission-track thermochronology to understand fault zones. In: Malusà MG, Fitzgerald PG (eds) Fission-track thermochronology and its application to geology. Springer, Berlin

Tagami T, Hasebe N, Kamohara H, Takemura K (2001) Thermal anomaly around the Nojima Fault as detected by fission-track analysis of Ogura 500 m borehole samples. Isl Arc 10(3–4):457–464

Thiede RC, Arrowsmith JR, Bookhagen B, McWilliams M, Sobel ER, Strecker MR (2006) Dome formation and extension in the Tethyan Himalaya, Leo Pargil, northwest India. Geol Soc Am Bull 118:635–650

Thomson SN (2002) Late cenozoic geomorphic and tectonic evolution of the Patagonian Andes between latitudes 42 S and 46 S: an appraisal based on fission-track results from the transpressional intra-arc Liquiñe-Ofqui fault zone. Geol Soc Am Bull 114:1159–1173

van der Beek P, Robert X, Mugnier JL, Bernet M, Huyghe P, Labrin E (2006) Late Miocene–recent exhumation of the central Himalaya and recycling in the foreland basin assessed by apatite fission-track thermochronology of Siwalik sediments, Nepal. Basin Res 18:413–434

Vermeesch P (2007) Quantitative geomorphology of the White Mountains (California) using detrital apatite fission track thermochronology. J Geophys Res Earth 112(F3)

Vermeesch P (2009) RadialPlotter: a Java application for fission track, luminescence and other radial plots. Rad Meas 44:409–410

Vermeesch P (2013) Multi-sample comparison of detrital age distributions. Chem Geol 341:140–146

Vermeesch P (2018) Chapter 6. Statistics for fission-track thermochronology. In: Malusà MG, Fitzgerald PG (eds) Fission-track thermochronology and its application to geology. Springer, Berlin

Villa IM, von Blanckenburg F (1991) A hornblende ^{39}Ar–^{40}Ar age traverse of the Bregaglia tonalite (southeast Central Alps). Schweiz Mineral Petrogr Mitt 71:73–87

Viola G, Mancktelow NS, Seward D (2001) Late Oligocene-Neogene evolution of Europe-Adria collision: new structural and geochronological evidence from the Giudicarie fault system (Italian Eastern Alps). Tectonics 20:999–1020

von Eynatten H, Dunkl I (2012) Assessing the sediment factory: the role of single grain analysis. Earth Sci Rev 115:97–120

Wagner GA, Reimer GM (1972) Fission track tectonics: the tectonic interpretation of fission track apatite ages. Earth Planet Sci Lett 14 (2):263–268

Wagner GA, Reimer GM, Jäger E (1977) Cooling ages derived by apatite fission track, mica Rb–Sr, and K–Ar dating: the uplift and cooling history of the central Alps. Mem Ist Geol Miner Univ Padova 30:1–27

Wagner GA, Miller DS, Jäger E (1979) Fission track ages on apatite of Bergell rocks from central Alps and Bergell boulders in Oligocene sediments. Earth Planet Sci Lett 45(2):355–360

Warren-Smith E, Lamb S, Seward D, Smith E, Herman F, Stern T (2016) Thermochronological evidence of a low-angle, mid-crustal detachment plane beneath the central South Island, New Zealand. Geochem Geophys Geosyst 17:4212–4235

West DP, Roden-Tice MK (2003) Late Cretaceous reactivation of the Norumbega fault zone, Maine: evidence from apatite fission-track ages. Geology 31(7):649–652

Willett SD, Fisher D, Fuller C, En-Chao Y, Chia-Yu L (2003) Erosion rates and orogenic-wedge kinematics in Taiwan inferred from fission-track thermochronometry. Geology 31:945–948

Wiltschko DV (1998) Analysis of veins in low temperature environments—introduction for structural geologists. Geol Soc Am. Short Course, 96 pp

Wittmann H, Von Blanckenburg F, Maurice L, Guyot JL, Kubik PW (2011) Recycling of Amazon floodplain sediment quantified by cosmogenic ^{26}Al and ^{10}Be. Geology 39(5):467–470

Wittmann H, Malusà MG, Resentini A, Garzanti E, Niedermann S (2016) The cosmogenic record of mountain erosion transmitted across a foreland basin: source-to-sink analysis of in situ ^{10}Be, ^{26}Al and ^{21}Ne in sediment of the Po river catchment. Earth Planet Sci Lett 452:258–271

Zanchetta S, Malusà MG, Zanchi A (2015) Precollisional development and Cenozoic evolution of the Southalpine retrobelt (European Alps). Lithosphere 7(6):662–681

Zattin M, Picotti V, Zuffa GG (2002) Fission-track reconstruction of the front of the Northern Apennine thrust wedge and overlying Ligurian unit. Am J Sci 302(4):346–379

Zattin M, Talarico FM, Sandroni S (2010) Integrated provenance and detrital thermochronology studies on the ANDRILL AND-2A drill core: late Oligocene-early miocene exhumation of the Transantarctic Mountains (southern Victoria Land, Antarctica). Terra Nova 22:361–368

Zwingmann H, Mancktelow N (2004) Timing of Alpine fault gouges. Earth Planet Sci Lett 223:415–425